SOME ASPECTS OF THE SOLUTION OF VECTOR TRANSFER EQUATION IN A MAGNETIZED MEDIUM

K. N. NAGENDRA and A. PERAIAH
Indian Institute of Astrophysics, Bangalore, India

(Received 5 June, 1985)

Abstract. A simplification of the numerical method of solving the vector transfer equation, given earlier by Nagendra and Peraiah (1985a), is described for problems which involve only absorption. This allows us to attempt to solve under realistic conditions and with reduced computing efforts, the important problems of polarization of light emerging from magnetized stars. For the purpose of illustration, the equations described are used for solving the continuum and Zeeman line transfer problems.

1. Introduction

The solutions of the transfer equation for polarized radiation are well known. For true absorption, the set of coupled transfer equations written for the polarization Stokes parameters admit an analytical solution. Various numerical methods have also been developed to obtain the solution to this problem (see Stenflo, 1971; Martin and Wickramasinghe, 1979b, for details and references). The simplest of all is the Unno solution which is derived analytically using a Milne–Eddington approximation. This solution is restricted, and cannot be used in computations involving realistic model atmospheres. The usual formal solution itself can be used as an alternative. For arbitrary source function gradients, and line formation problems, the depth integration, however, requires a large number of grid points. Among the numerical solutions the most accurate and widely used is the Beckers' method, which is a Runge–Kutta scheme for the vector transfer equation. For a detailed discussion on the accuracy and computing times of some of the numerical solutions, see Martin and Wickramasinghe (1979b) and Nagendra and Peraiah (1985a). In the computations of spectra and polarizations of magnetic stars (Ap stars, white dwarfs, etc.), we are required to solve the transfer equation over a large number of points on the disk and finally to integrate these local solutions along the line-of-sight. This is a highly time-consuming but unavoidable process, particularly so in line computations where large numbers of frequency points are also involved. In view of this difficulty, one is forced to use quicker but less accurate methods. We have previously described a procedure based on the discrete space theory (hereafter called DSM) of radiative transfer (Nagendra and Peraiah, 1985a). In this paper we describe a simplification of the same work, which is quicker, and present the results of computations using these equations.

2. Matrix Formal Solution and its Relation to the DSM Solution

The matrix transfer equation in a plane-parallel stratification for the polarized radiation

Astrophysics and Space Science **117** (1985) 121–135. 0004–640X/85.15

field is given in usual notation by

$$\mathbf{M}\frac{\mathrm{d}\mathbf{I}}{\mathrm{d}\tau} = \mathbf{A}(\mathbf{I} - \mathbf{B}), \tag{1}$$

where

$$\mathbf{M} = \begin{matrix} \mu & & \\ & \mu & \\ & & \mu \end{matrix}; \quad \mathbf{A} = \begin{matrix} \eta_I & \eta_Q & 0 & \eta_V \\ \eta_Q & \eta_I & -\rho_R & 0 \\ 0 & \rho_R & \eta_I & -\rho_W \\ \eta_V & 0 & \rho_W & \eta_I \end{matrix}, \tag{2}$$

and

$$\mathbf{I} = (I\ Q\ U\ V)^T; \qquad \mathbf{B} = (B\ 0\ 0\ 0)^T,\ B = B_\nu(T), \tag{3}$$

which is an 'ordinary matrix differential equation'. The boundary conditions are given at the bottom and the top of the stellar atmosphere,

$$\mathbf{I}(0, \mu) = \mathbf{g}; \qquad \mathbf{I}(\tau_{\max}, \mu) = \mathbf{h}. \tag{4}$$

The transfer matrix **A** has the following characteristics:
(i) it is symmetric Hermitian when $\rho_R = \rho_W \equiv 0$, but not otherwise;
(ii) diagonal elements are always positive, and in the special case of very weak anisotropy, **A** is diagonally dominant also;
(iii) by a proper choice of coordinate system **A** can be diagonalized;
(iv) it is irreducible, because, by any set of transformations, it is not possible to reduce it to the upper triangular form.

Equation (1) can be written in the half-space of angles $\mu \in (0, 1)$, as

$$-\mathbf{M}\frac{\mathrm{d}\mathbf{I}^-}{\mathrm{d}\tau} = \mathbf{A}^-(\mathbf{I}^- - \mathbf{B}^-), \tag{5}$$

$$\mathbf{M}\frac{\mathrm{d}\mathbf{I}^+}{\mathrm{d}\tau} = \mathbf{A}^+(\mathbf{I}^+ - \mathbf{B}^+), \tag{6}$$

with $\mathbf{I}^- = \mathbf{I}(\tau, -\mu)$ and $\mathbf{I}^+ = \mathbf{I}(\tau, \mu)$ representing the rays emerging towards the surface of a star and entering into the atmosphere, respectively. In the integration of the transfer equation over an elementary 'cell', **I**, **B**, and **A** can be taken as constant, being some sort of average of these quantities at the boundaries of the cell, bounded by the planes τ_n and τ_{n+1}, $n = 1, 2, 3, \ldots$ (Peraiah and Varghese, 1985; Nagendra and Peraiah, 1985a). The formal solutions of Equations (5) and (6) can be written as

$$\mathbf{I}_n^- = \mathbf{I}_{n+1}^- \exp[-\Delta\tau\mathbf{M}^{-1}\mathbf{A}^-] + \int_{\tau_n}^{\tau_{n+1}} \exp[-(t - \tau_n)\mathbf{M}^{-1}\mathbf{A}^-]\mathbf{M}^{-1}\{\mathbf{A}^-\mathbf{B}\}\,\mathrm{d}t \tag{7}$$

for the outgoing ray, and

$$\mathbf{I}^{+}_{n+1} = \mathbf{I}^{+}_{n} \exp[-\Delta\tau\mathbf{M}^{-1}\mathbf{A}^{+}] + \int_{\tau_n}^{\tau_{n+1}} [-(\tau_{n+1} - t)\mathbf{M}^{-1}\mathbf{A}^{+}]\mathbf{M}^{-1}\{\mathbf{A}^{+}\mathbf{B}\}\, dt \tag{8}$$

for the incoming ray. $\Delta\tau = \tau_{n+1} - \tau_n$, $n = 1, 2, \ldots, N$, where N = number of layers. $\{\mathbf{A}^{\pm}\mathbf{B}\}$ is the source function. For the present discussion, we shall concentrate on only the outgoing ray (7). Now, assuming that $\{\mathbf{A}^{\pm}\mathbf{B}\}$ is independent of optical depth – that is, it remains constant in the range τ_n to τ_{n+1} – we get, by performing the integral in Equation (7),

$$\mathbf{I}^{-}_{n} = \mathbf{B} + \exp[-\Delta\tau\mathbf{M}^{-1}\mathbf{A}^{-}] \cdot \{\mathbf{I}^{-}_{n+1} - \mathbf{B}\}, \tag{9}$$

which is the usual formal solution and, again, demands no restriction on $\Delta\tau$ as long as the physical properties remain constant in the range of integration.

Now, we descritize the matrix transfer equation (1) by directly integrating it over an elementary cell as before. We then obtain

$$\pm \mathbf{M}[\mathbf{I}^{\pm}_{n+1} - \mathbf{I}^{\pm}_{n}] = \tau_{n+\frac{1}{2}}\mathbf{A}^{\pm}_{n+\frac{1}{2}}[\mathbf{I}^{\pm}_{n+\frac{1}{2}} - \mathbf{B}_{n+\frac{1}{2}}], \tag{10}$$

where the subscript $(n + \frac{1}{2})$ refers to the average of the values of physical variables at τ_n and τ_{n+1}. For the diamond difference scheme, we have

$$\mathbf{I}^{\pm}_{n+\frac{1}{2}} = \frac{\mathbf{I}^{\pm}_{n+1} + \mathbf{I}^{\pm}_{n}}{2}; \qquad \tau_{n+\frac{1}{2}} = \Delta\tau_n = \tau_{n+1} - \tau_n, \text{ etc.}, \tag{11}$$

which assumes that the intensity is linear in optical depth within the cell. For further details on the method of solution, see Peraiah (1984) and Nagendra and Peraiah (1985a). Restricting ourselves to the outgoing ray, we have, from DSM, the following expressions for the outward-directed ray:

$$\mathbf{I}^{-}_{n} = \mathbf{t}^{-}\mathbf{I}^{-}_{n+1} + \tau_{n+\frac{1}{2}}\Delta^{-}\mathbf{A}^{-}_{n+\frac{1}{2}}\mathbf{B} = \mathbf{t}^{-}\mathbf{I}^{-}_{n+1} + \mathbf{\Sigma}^{-}, \tag{12}$$

where

$$\mathbf{t}^{-} = \Delta^{-}\mathbf{S}^{-}, \tag{13}$$

$$\Delta^{-} = [\mathbf{M} + \tfrac{1}{2}\tau_{n+\frac{1}{2}}\mathbf{A}^{-}_{n+\frac{1}{2}}]^{-1}, \tag{14}$$

$$\mathbf{S}^{-} = [\mathbf{M} - \tfrac{1}{2}\tau_{n+\frac{1}{2}}\mathbf{A}^{-}_{n+\frac{1}{2}}]. \tag{15}$$

Now expanding the Δ^{-} matrix (Equation (14)) in a matrix power series, then substituting in Equation (12) and truncating the resulting expansion to the quadratic terms, we get

$$\mathbf{I}^{-}_{n} \simeq \mathbf{I}^{-}_{n+1} - \tau_{n+\frac{1}{2}}\mathbf{M}^{-1}\mathbf{A}^{-}_{n+\frac{1}{2}}[\mathbf{I}^{-}_{n+1} - \mathbf{B}_{n+\frac{1}{2}}] + \tfrac{1}{2}\tau^{2}_{n+\frac{1}{2}}\{(\mathbf{M}^{-1}\mathbf{A}^{-}_{n+1})^{2}[\mathbf{I}^{-}_{n+1} - \mathbf{B}_{n+\frac{1}{2}}]\} - \cdots. \tag{16}$$

Now imposing an asymptotic boundary condition, like the Unno solution

$$(\mathbf{I}^{-}_{N+1})_{\mathrm{U}} = \mathbf{B}_{N+1} + \mathbf{M}[\mathbf{A}^{-}_{N+1}]^{-1}\boldsymbol{\beta}\,; \qquad \boldsymbol{\beta} = \left.\frac{\mathrm{d}\mathbf{B}}{\mathrm{d}\tau}\right|_{N+1}, \tag{17}$$

at the lower boundary $(N+1)$ of the stellar atmosphere, we can get the emergent intensity recursively ($n = N, N-1, \ldots, 1$) using Equation (16). It is more useful when the source function is a linear or a nearly linear function of τ and the linear perturbation vector $\boldsymbol{\beta}$ is weak. In that case, we can substitute an Unno solution at each grid point n and, assuming a constancy of opacity and source function in each cell, get a relation of the form

$$\mathbf{I}^{-}_{n} \simeq (\mathbf{I}^{-}_{n})_{\mathrm{U}} - \boldsymbol{\beta}\tau_{n+\frac{1}{2}} + \tfrac{1}{2}\mathbf{M}^{-1}\mathbf{A}^{-}_{n+\frac{1}{2}}\boldsymbol{\beta}\tau^{2}_{n+\frac{1}{2}} - \cdots . \tag{18}$$

When $\boldsymbol{\beta} \ll \tau_{n+\frac{1}{2}}\mathbf{1}$, this equation is stable and gives an accurate and convergent solution even for step sizes $\tau_{n+\frac{1}{2}} = \Delta\tau_n > 1$. In practice, we can use the nodal points of the tabulated stellar atmospheric model themselves as the grid points for constructing the cells, because in the deeper 'thicker' layers of the model the $\boldsymbol{\beta}$ parameter will be very small, and in the upper layers, where $\boldsymbol{\beta}$ could be larger, the nodal point spacing would be very small (i.e. $\tau_{n+\frac{1}{2}} \ll 1$), making the solution (18) still correct. Notice, however, that the original DSM equation (12) is simply the implicit Crank–Nicolson matrix approximation for $\exp[-\frac{1}{2}\tau_{n+\frac{1}{2}}\mathbf{M}^{-1}\mathbf{A}^{-}_{n+\frac{1}{2}}]$ in solving the inhomogeneous parabolic matrix differential equation (1). It is well known that the Crank–Nicolson scheme is second-order accurate, unconditionally stable, and a consistent approximation for all step sizes, since $\mathrm{Re}\,\lambda_i > 0$ (see Varga, 1963; p. 270), where $\lambda_i = a_{i,\,n+\frac{1}{2}}/\mu$ $(i = 1, 2, 3, 4)$ are the eigenvalues of $\mathbf{M}^{-1}\mathbf{A}^{-}_{n+\frac{1}{2}}$. a_i are the eigenvalues of the transfer matrix $\mathbf{A}^{-}$, with two of them being complex in general.

It can be clearly seen from Equations (12)–(15) that the central difference approximation to the transmission matrix $\mathbf{t}^{-}$ is a matrix power series approximation for the matrix exponential $\exp[-\tau_{n+\frac{1}{2}}\mathbf{M}^{-1}\mathbf{A}^{-}_{n+\frac{1}{2}}]$ through quadratic terms. Similarly, $\boldsymbol{\Delta}^{-}$ is a backward difference approximation to the same matrix exponential through linear terms, again being unconditionally stable. Thus, we can write Equation (12) to the lowest order approximation as

$$\mathbf{I}^{-}_{n} \simeq \exp[-\tau_{n+\frac{1}{2}}\mathbf{M}^{-1}\mathbf{A}^{-}_{n+\frac{1}{2}}]\,[\mathbf{I}^{-}_{n+1} + \tau_{n+\frac{1}{2}}\mathbf{M}^{-1}\mathbf{A}^{-}_{n+\frac{1}{2}}\mathbf{B}]\,, \tag{19}$$

and we see that the right-hand side of this equation is convergent even for $\tau_{n+\frac{1}{2}} \geq 1$. This is a consequence of the approximation of linear variation of the source function with optical depth (implied in the use of the diamond scheme). This has the important property of causing the calculated intensities to be correct in the 'diffusion limit'. Grant (1963) has shown in this regard that the difference equations of DSM naturally reduce to the difference analogue of the diffusion equation (see, e.g., Equation (18)), in the limit of large $\tau_{n+\frac{1}{2}}$. This property is lost if one assumes a constant source function throughout the atmosphere (see Wiscombe, 1976) or if the source function is a highly nonlinear function of optical depth. Obviously, this property of DSM equations provides large

practical advantages, particularly in the work with stellar atmospheres like those of white dwarfs. In the following section we show the results obtained using this criterion for the problems of continuum and line polarization, using realistic model atmospheres. Since our primary interest in such computations is only the emergent (at $\tau = 0$) values of $\mathbf{I}^-$, the following simplified form of the conventional DSM equations, namely

$$\mathbf{t}^-(1, N) = \mathbf{t}^-(1) \cdot \mathbf{t}^-(2) \cdot \mathbf{t}^-(3) \cdot \mathbf{t}^-(4) \cdot \ldots \cdot \mathbf{t}^-(N-1) \cdot \mathbf{t}^-(N)\,, \tag{20}$$

and

$$\begin{aligned}\boldsymbol{\Sigma}^-(1, N) = {} & \boldsymbol{\Sigma}^-(1) + \mathbf{t}^-(1) \cdot \boldsymbol{\Sigma}^-(2) + \mathbf{t}^-(1) \cdot \mathbf{t}^-(2) \cdot \boldsymbol{\Sigma}^-(3) \\ & + \mathbf{t}^-(1) \cdot \mathbf{t}^-(2) \cdot \mathbf{t}^-(3) \cdot \boldsymbol{\Sigma}^-(4) + \cdots + \\ & + \mathbf{t}^-(1) \cdot \mathbf{t}^-(2) \cdot \ldots \cdot \mathbf{t}^-(N-1) \boldsymbol{\Sigma}^-(N)\,,\end{aligned} \tag{21}$$

can be used. N, here, is the total number of atmospheric layers considered from the model atmosphere. Though diffusion approximation places no restriction on the step size, we can use $\tau_{n+\frac{1}{2}} \simeq 2$ as a safe choice in computing the $\mathbf{t}^-$ and $\boldsymbol{\Sigma}^-$ matrices of the respective layers (see Kalkofen and Wehrse, 1982a, b). These authors have made an extensive analysis of the finite difference techniques in general. Our Equation (12) is, for example, the polarized analogue of their Equation (25) in their (1982a) paper with a half-implicit differencing weight. The thick layer operators can be generated by the usual doubling algorithm (Grant and Hunt, 1969; Peraiah, 1984). We have repeated some of the test cases – Tables (1)–(4) of Nagendra and Peraiah (1985a) – now using the diffusion approximation described in the previous section (Equations (12), (17), (20), and (21)). Since the agreement is good up to the third or fourth digits, we do not repeat them here. Instead, we describe the line formation under arbitrary physical conditions, using a model atmosphere taken from Wehrse (1976), and the opacity parameters representative of a cold, weak field ($H \sim 3 \times 10^5$ G) magnetic white dwarf. In addition, the following two tests – namely, $\psi(\tau) = (0, \pi)$ with $\psi(0) = 0$, $\psi(\tau_{\max}) = \pi$ for $\chi = 0$ should give $Q(0) = U(0) \equiv 0$, and $\chi(\tau) = (0, 2\pi)$ with $\chi(0) = 0$, $\chi(\tau_{\max}) = 2\pi$ for $\psi = \pi/2$ should give $U(0) = V(0) \equiv 0$ – are satisfied exactly, confirming that no spurious sources or sinks are introduced by the diffusion approximation, even in a realistic atmosphere.

3. Application to the Zeeman Line Formation under General Physical Conditions and Continuum Polarization Problems

The transfer coefficients of the **A** matrix in Equation (2) are given by

$$\begin{aligned}\eta_I &= \tfrac{1}{2}\eta_p \sin^2\psi + \tfrac{1}{4}(\eta_l + \eta_r)(1 + \cos^2\psi)\,, \\ \eta_Q &= \tfrac{1}{2}\eta_p \sin^2\psi - \tfrac{1}{4}(\eta_l + \eta_r)\sin^2\psi\,, \\ \eta_U &= 0\,, \\ \eta_V &= \tfrac{1}{2}(\eta_r - \eta_l)\cos\psi\,.\end{aligned} \tag{22}$$

ψ is the angle between the ray and the magnetic field. If the solution for an arbitrary azimuth χ is required, it can be obtained by rotating the solution vector using the transformation matrix for $(QU)^T$, namely

$$\begin{bmatrix} \cos 2\chi & -\sin 2\chi \\ \sin 2\chi & \cos 2\chi \end{bmatrix}. \tag{23}$$

For the purpose of discussion, retaining the picture of a triplet, we have,

$$\eta_i = \eta_i^C + \eta_i^L = \eta_i^C + \eta_0 H(a, v - v_i), \quad i = p, l, r, \tag{24}$$

where

$$v_i = \frac{v_i - v_0}{\Delta v_D}, \qquad \Delta v_D = \frac{v_0}{c}\sqrt{\frac{2kT}{M}}; \tag{25}$$

in which a is the damping constant; v_i $(i = p, l, r)$ are the central frequencies of the $\Delta M = 0, \pm 1$ transitions, respectively; η_0 is the line centre absorption coefficient for zero damping $(a = 0)$; and

$$\rho_R = \rho_R^C + \rho_R^L = -\frac{\omega_0^2 \omega_c \cos\psi}{ck^C(\omega^2 - \omega_c^2)} - \\ - \eta_0[F(a, v - v_r) - F(a, v - v_l)] \cos\psi, \tag{26}$$

$$\rho_W = \rho_W^C + \rho_W^L = -\frac{\omega_0^2 \omega_c \sin^2\psi}{2c\omega k^C(\omega^2 - \omega_c^2)} - \\ - \eta_0[F(a, v - v_p) - \tfrac{1}{2}\{F(a, v - v_l) + F(a, v - v_r)\}] \sin^2\psi; \tag{27}$$

$\omega_0 = \sqrt{4\pi N_e e^2/m_e}$ being the plasma frequency and $\omega_c = eH/m_e c$ the cyclotron frequency. The Voigt and plasma dispersion functions are given by

$$H(a, u) = \frac{a}{\pi}\int_{-\infty}^{+\infty} \frac{\exp[-(y + u)^2]}{y^2 + a^2}\, dy,$$

$$F(a, u) = \frac{1}{2\pi}\int_{-\infty}^{+\infty} \frac{y \exp[-(y - u)^2]}{y^2 + a^2}\, dy, \tag{28}$$

with $H(a, u) = H(a, -u)$; $F(a, u) = -F(a, -u)$. We can use the following useful relations (cf. Heinzel, 1978)

$$F(a, u) = \frac{1}{a}\left[\frac{1}{2} uH(a, u) + \frac{1}{4}\frac{d}{du} H(a, u)\right], \tag{29}$$

or

$$F(a, u) = \frac{1}{a} \left[\tfrac{1}{2} u H(a, u) + \tfrac{1}{2}\{K(a, u)a - H(a, u)u\}\right] . \tag{30}$$

Therefore,

$$F(a, u) = \frac{1}{2} K(a, u) = \frac{1}{2\pi} \int_{-\infty}^{+\infty} \frac{y \exp[-(y-u)^2]}{y^2 + a^2} \, dy . \tag{31}$$

The H and K functions can be computed by fast algorithms given by Matta and Reichel (1971).

The Stokes parameter profiles arising due to the linear Zeeman effect and anomalous dispersion in the line preserve a symmetry (for I, Q, and U) or an antisymmetry (for V) about the line centre. Many authors have computed such profiles – Beckers (1969), Stenflo (1971), Landi Degl'Innocenti (1979), and Wittmann (1974) to mention only few. In the strong magnetic fields, higher-order magnetic perturbations (quadratic Zeeman effect) or electric perturbations (Stark effects which can cause large asymmetries) affect the Zeeman line profiles (Nagendra and Peraiah, 1985b). Apart from this, the macroscopic mass motions, stellar rotation, and gravitational redshift can also produce asymmetric Stokes profiles. All such geometrical effects can easily be included in a unified way for the computations of pure absorption lines. If the macroscopic velocity vector $u_m(\tau)$ makes an angle $\alpha(\tau)$ w.r.t. the line-of-sight, the Doppler shift of the line centre frequency in the rest frame of the star is given by

$$\nu_0(\tau) = \nu_0 + \cos\alpha(\tau) \frac{u_m(\tau)}{c} \nu_0 , \tag{32}$$

from which we can get, for any frequency ν in the line

$$v(\tau) = v - \cos\alpha(\tau) \frac{u_m(\tau)}{c} \frac{\nu_0}{\Delta\nu_D} , \tag{33}$$

where

$$v(\tau) = \frac{\nu - \nu_0(\tau)}{\Delta\nu_D} ; \qquad v = \frac{\nu - \nu_0}{\Delta\nu_D} ; \qquad \Delta\nu_D = \frac{\nu_0}{c} u_T . \tag{34}$$

Expressing the velocity $u_m(\tau)$ in terms of some standard mean thermal units (m.t.u.) u_T, we have

$$v(\tau) = v - \cos\alpha(\tau) V_m(\tau) , \tag{35}$$

where $V_m(\tau) = u_m(\tau)/u_T$ is the dimensionless parameter. When the continuum is taken to be polarized and magneto-optic, the Stokes profiles are basically asymmetric since both the absorption and dispersion coefficients do not preserve symmetry about the line centre.

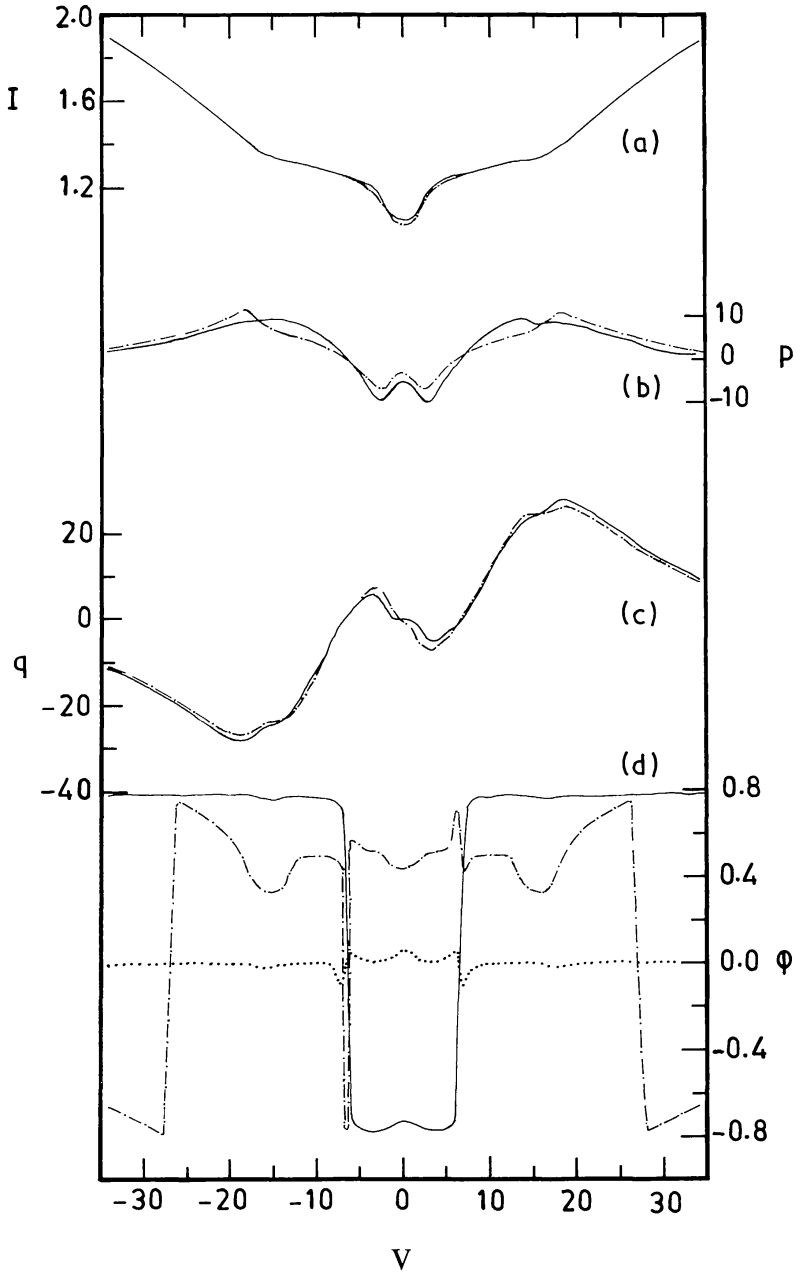

Fig. 1. Intensity (a), percentage linear polarization (b), percentage circular polarization (c), and polarization position angle (d) for a hypothetical Zeeman triplet. $v = \Delta v/\Delta v_D$ and $v_p = 0$, $v_l = 16$, $v_r = -16$. $a = 0.1$ and $\mu = 0.8$. The continuous dichroism introduced via $\eta_p = 1.00$, $\eta_l = 0.94$, $\eta_r = 1.1$, while $\eta_0(a = 0, v = 0) = 10^4$ for a line of wavelength $\lambda(v = 0) = 5000$ Å. $\rho_R^C = -10 \cos\psi$ and $\rho_W^C = -0.25 \sin^2\psi$. These parameters are typical of a weak line formed in a cool, high-gravity white dwarf atmosphere. A hydrogen-rich convective equilibrium model with $T_{\text{eff}} = 9000$ K, $\log g = 8$, from Wehrse (1976) is adopted. The full drawn profiles represent Case x: $\psi = \pi/4$, $\chi = \pi/4$, i.e. field orientation independent of depth. Dot–dash profiles, $\psi = \pi/4$, $\chi = \chi(\tau)$, i.e. azimuth variation; and dotted lines, $\psi = \pi/4$, $\chi = 0$.

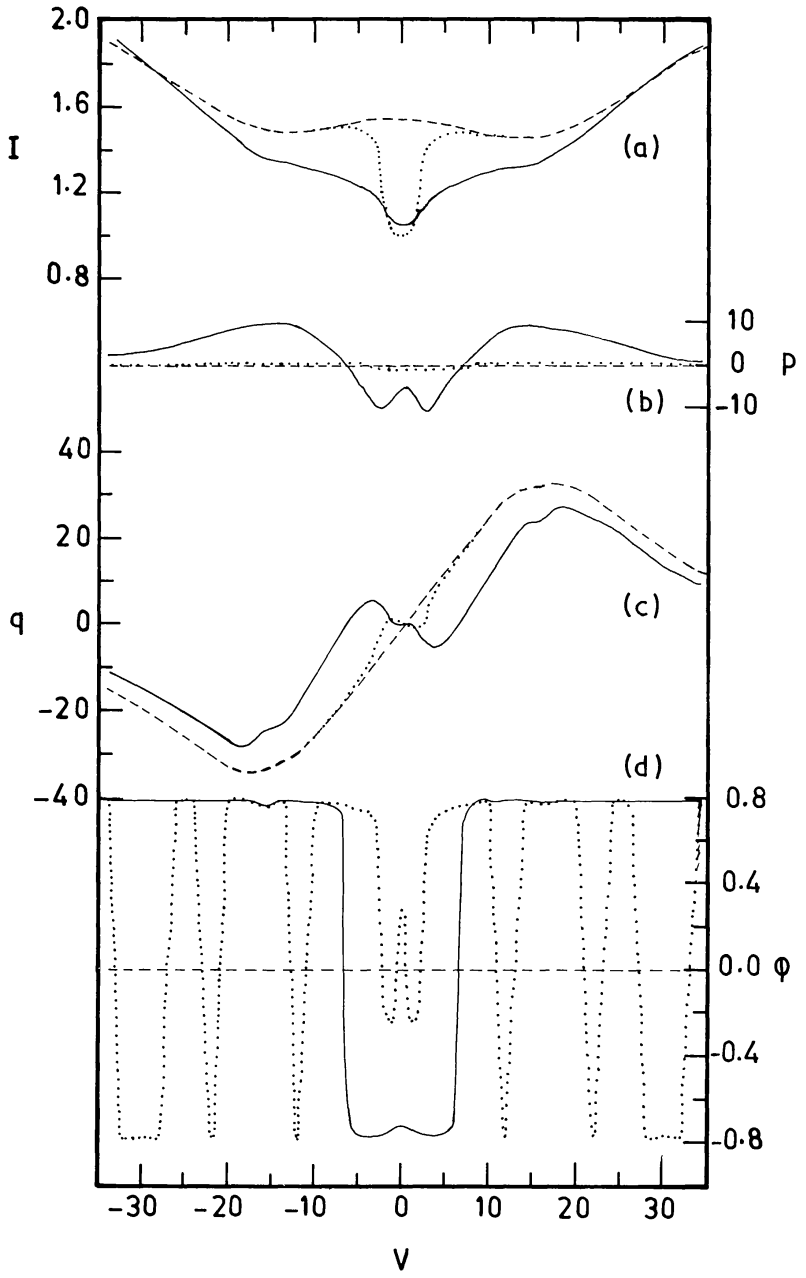

Fig. 2. As Figure 1, but showing the following cases. Full lines, Case x; dashed lines, $\psi = 0$, $\chi = 0$; dotted lines, $\psi = \psi(\tau)\chi = \pi/4$, i.e. ψ variation.

In Figures 1 to 4 we show the changes produced by taking some of the parameters as depth dependent. Figure 1 shows the effect of azimuth variation. The solid curves show the Stokes profiles for a depth independent field direction ($\psi = \pi/4$; $\chi = \pi/4$) w.r.t. the line-of-sight, which we shall refer to as Case x. The I, p, and q profiles for $\psi = \pi/4$, $\chi = 0$ are the same as for Case x because of the complementary nature of the azimuth angles $\pi/4$ and 0. The dotted line in (d) for this later case shows the position angle ϕ

TABLE I

Disk-integrated linear ($\bar{p}$) and circular ($\bar{q}$) polarization from a magnetic white dwarf for two wavelengths. i is the inclination of the dipole axis to the sight line. $\rho_R = \rho_W \equiv 0$ for all the cases

		λ = 3500 Å		λ = 4500 Å	
		$\bar{p}$ ($\times 10^{-5}$)	$\bar{q}$ ($\times 10^{-3}$)	$\bar{p}$ ($\times 10^{-5}$)	$\bar{q}$ ($\times 10^{-3}$)
$i = 0°$	MW	0.00	−4.90	0.00	−5.30
	DA	0.00	−4.85	0.00	−5.27
$i = 45°$	MW	2.50	−3.50	4.20	−3.70
	DA	2.12	−3.43	3.78	−3.66
$i = 90°$	MW	5.10	0.00	8.40	0.00
	DA	4.76	0.00	7.95	0.00

is quite small throughout the profile and arises only because of the magneto-optical effects. We have included the depth dependence of the azimuth angle χ in the transfer equation through replacing ρ_R by $\rho_R - 2\mu\,(\mathrm{d}\chi(\tau)/\mathrm{d}\tau)$. A small variation represented by $\chi(\tau) = (\pi/16)\exp(-\tau)$ is used. The intensity (dot–dash profiles) is not greatly affected except in the core. The p profile equivalent width increases and its central depth is reduced. The q profile is affected to a larger extent only near the π component of the triplet. The sharp changes in the position angle ϕ near $v \sim 7$ are because the Q and U parameters simultaneously change sign in this region (see also Staude, 1970). Recently, Deguchi and Watson (1985) have computed the Zeeman lines formed in such a twisting magnetic field. The Stokes profiles in Figure 1 are in agreement with their 'optically thick' lines.

Figure 2 shows the changes produced by the depth variation of ψ. For the case $\psi = 0$, $\chi = 0$ (indicated by dashed lines), we can see that the σ components are clearly stronger and the π component is absent; $p = 0$ and $\phi = 0$. The q profile does not show the 'π component splitting' indicating that 'coupling of the Stokes parameters' is necessary for such a splitting along with the usual magneto-optical effects (e.g. Case x: solid line). The variation of the angle ψ as $\psi(\tau) = (\pi/16)\exp(-\tau)$ has definite effects on the I, q, and ϕ profiles ($\psi = \psi(\tau)$, $\chi = \pi/4$: dotted lines). The ϕ profile undergoes fluctuations because of a strong coupling of the V parameter to Q and U through magneto-optical effects and a changing inclination (see Beckers, 1969). p also fluctuates, but is unresolved in the figure since it is smaller in magnitude.

In Figure 3 we show a combination of the simultaneous variation of ψ and χ along with a variation in field strength according to the formula $v_H(\tau) = 16\{1 + 0.1(1 - \exp(-\tau))\}$, $(+v_l = -v_r \equiv v_H(\tau))$. From the profiles (dashed lines), it is seen that in the core of the line the ψ variation dominates while in the wings the χ variation is important in the line formation. The effect of an inhomogeneous (depth dependent) field is marginal compared to the changes produced by angular variations. Case x is also shown for comparison in this figure.

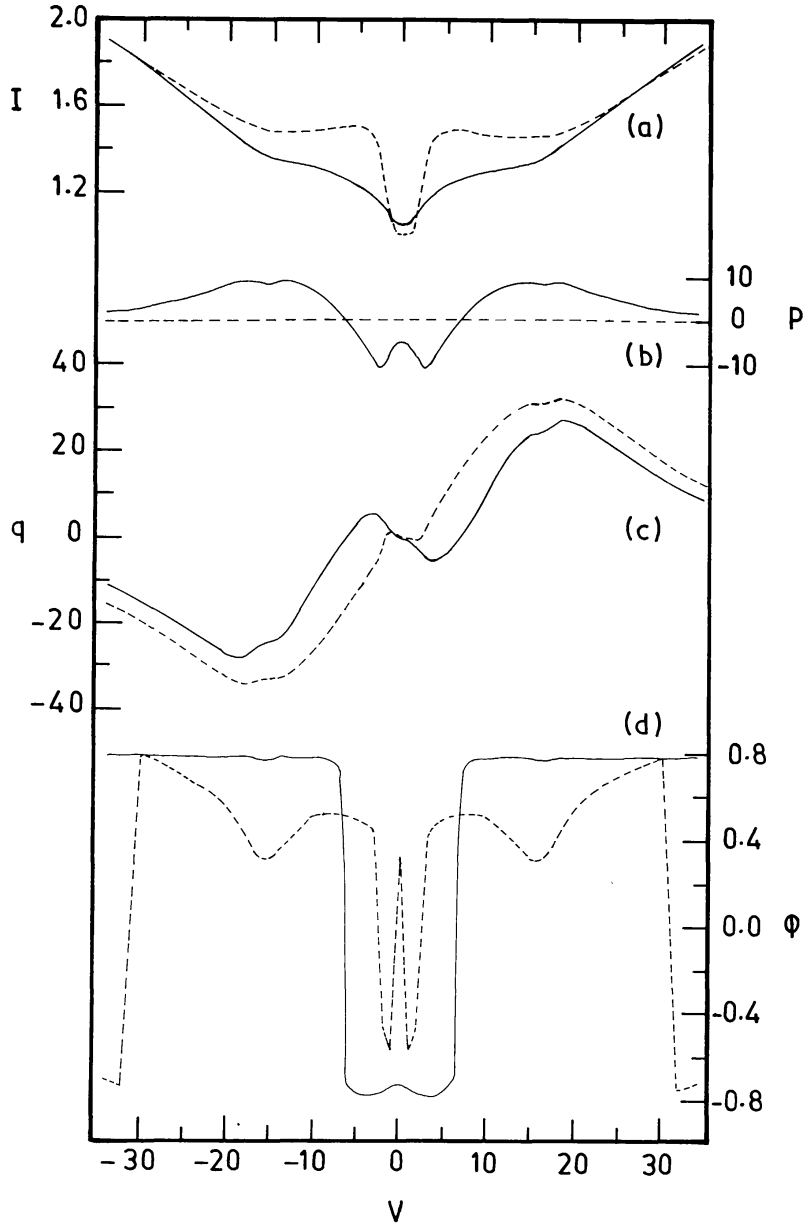

Fig. 3. As Figure 1, but with the following cases. Full lines, Case x; dashed lines, $\psi = \psi(\tau)$, $\chi = \chi(\tau)$, $H = H(\tau)$, i.e. changing orientation of the field vector. The case $\psi = \pi/4$, $\chi = \pi/4$, $H = H(\tau)$ is indistinguishable from Case x.

In Figure 4 we show the profiles formed in quite general situations. The dotted lines are the profiles formed in an arbitrarily moving atmosphere represented by $v(\tau) = 0.2 + 0.1(1 + \exp(-\tau))$, $\alpha(\tau) = \cos^{-1}\mu + (\pi/16)\exp(-\tau)$, with the magnetic field also being taken as inhomogeneous. It can be seen that the field gradient enhances the asymmetry near the line centre and reduces the same in the wings. The full lines are the profiles when there is a change in the angles ψ and χ only (see, e.g., Figure 3). The dashed lines represent the most general case of the profiles formed in arbitrarily varying

angles, velocity, and magnetic fields which, excepting a small asymmetry, are not very different from the former case (full lines). Thus, when the line shift asymmetries are weaker, the angular variation of the field vector is a dominant mechanism which can change the shape of the polarization profiles.

Apart from treating the sensitive, line formation problems, as a further test on the usefulness of the diffusion approximation we have computed the continuum linear and

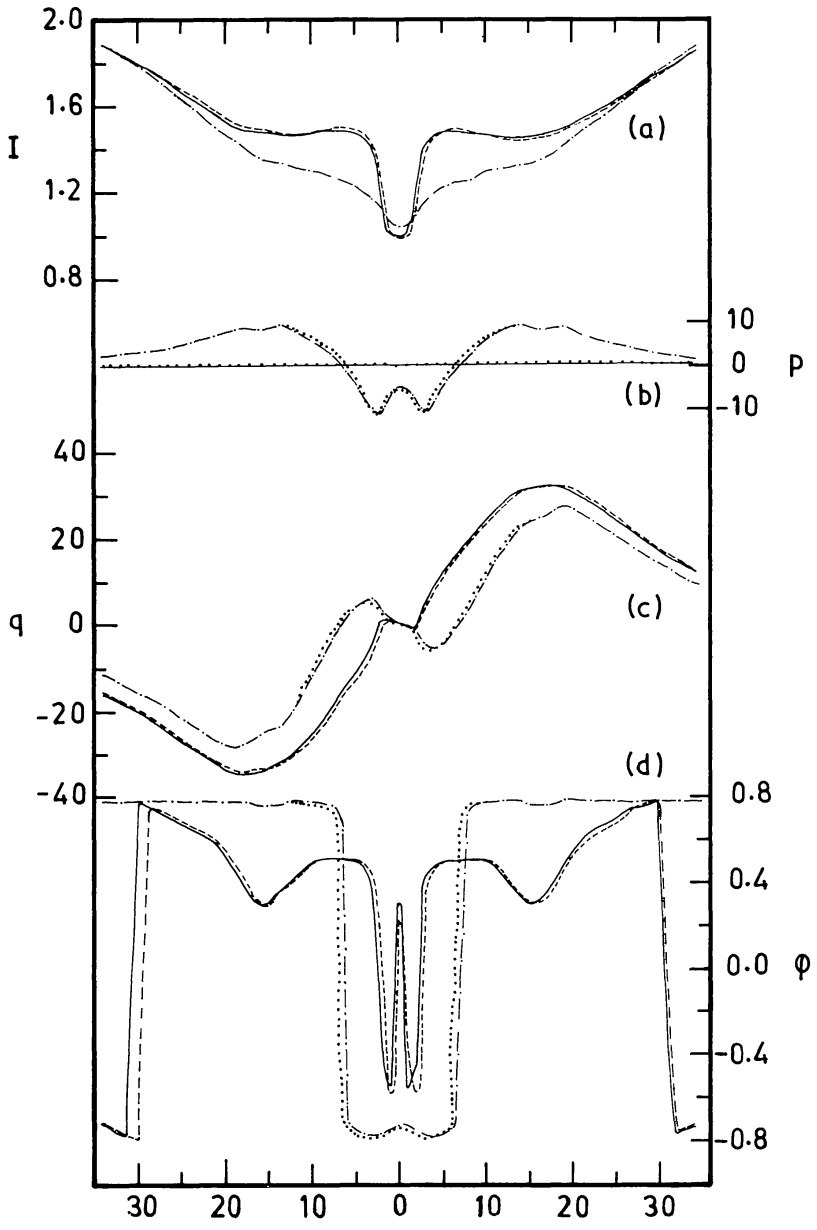

Fig. 4. As Figure 1, but showing the line profiles in an arbitrarily varying velocity and magnetic vectors. Dash–dot lines: Case *x*. Dotted lines: $\psi = \pi/4$, $\chi = \pi/4$, $V_m = V_m(\tau)$, $\alpha = \alpha(\tau)$, $H = H(\tau)$. Full lines: $\psi = \psi(\tau)$, $\chi = \chi(\tau)$, i.e. changing orientation of only the magnetic vector. Dashed lines: $\psi = \psi(\tau)$, $\chi = \chi(\tau)$, $V_m = V_m(\tau)$, $\alpha = \alpha(\tau)$, $H = H(\tau)$, i.e. the most general case of varying velocity and the field vectors.

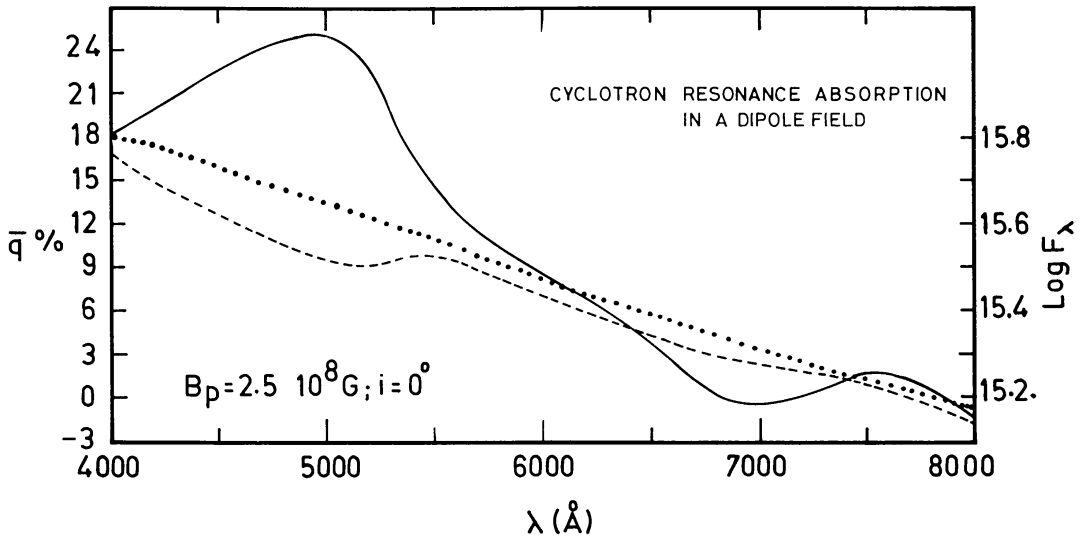

Fig. 5. The disk-integrated circular polarization $\bar{q}$ (full line) and spectra (dashed line) in a strong field white dwarf. The non-magnetic spectra is shown by the dotted line. The linear polarization $\bar{p} \equiv 0$, by symmetry. A $T_{\text{eff}} = 9000$ K, $\log g = 8$, radiative model is adopted from Wehrse (1976).

circular polarization in a magnetic white dwarf atmosphere with a central dipole field of polar strength $H_p = 10^7$ G. A model atmosphere of $T_{\text{eff}} = 20\,000$ K, $\log g = 8$, taken from Wickramasinghe (1972) is used. The continuum polarization is included according to Nagendra and Peraiah (1984). The specific intensity vectors are computed on 256 points on the visible disk of a white dwarf for a given angle of inclination (i) of the dipole axis to the line-of-sight. Equations (20)–(22) have been used for this purpose. The disk integration is performed using a 16-point Gaussian quadrature formula. For a few cases we have compared our results (referred to as DA = diffusion approximation) with the solutions obtained by Martin and Wickramasinghe (1982) presented in Table 1 of their paper (referred to as MW). The linear polarization is extremely small and no great significance can be placed on it unless it is much larger.

One more highly time-consuming problem, when computed using the conventional step size criterion $\tau_{n+\frac{1}{2}} \leq \min(2\mathbf{MA}^{-1}_{n+\frac{1}{2}})$, is the polarization arising due to cyclotron resonance absorption. The importance of this mechanism, particularly for magnetic white dwarfs, was emphasized by Lamb and Sutherland (1974); Gnedin and Sunyaev (1974), Landstreet and Angel (1975), and Pavlov and Shibanov (1978). Some characteristics of cyclotron absorption in realistic situations has been discussed extensively by Martin and Wickramasinghe (1979a). We have used the Lamb–Sutherland formula

$$\eta_r = \frac{4\pi^{3/2}}{\omega}\left(\frac{e^2}{m_e c}\right)\left(\frac{N_e}{k^C}\right)\left[\frac{m_e c^2}{2kT\cos^2\psi}\right]^{1/2} \times$$

$$\times\left[1 - \exp\left(-\frac{\hbar\omega}{kT}\right)\right]^{-1} \exp\left[-\frac{m_e c^2(\omega - \omega_c)^2}{2kT\omega^2\cos^2\psi}\right], \tag{36}$$

in the Doppler core, and the larger of the above and the collisionally damped absorption coefficient

$$\eta_r = \left(\frac{e^2}{m_e c}\right)\left(\frac{N_e}{k^C}\right)\left(\frac{kT}{2\pi\hbar\omega}\right)(1 + \cos^2\psi) \times$$

$$\times \left[\frac{\nu_{\text{coll}}}{(\omega - \omega_c)^2 + \nu_{\text{coll}}^2}\right]\left[\exp\left(\frac{\hbar\omega}{kT}\right) - 1\right], \tag{37}$$

due to Bekefi (1966), in the Lorentz wings of the Voigt profile of resonance. The collisional frequency can be calculated using

$$\nu_{\text{coll}} = \frac{\omega_0^2 e^2}{m_e V_e^3}\ln\Lambda\,; \qquad V_e = \sqrt{\frac{2kT}{m_e}}\,; \qquad \ln\Lambda \simeq 9.1 - \frac{\ln N_i}{2} + \frac{3}{2}\ln T, \tag{38}$$

from Melrose (1980). The nature of the spectrum and polarization depend quite strongly on the viewing angle, because of strong anisotropy of the radiation field. In Figure 5 we have shown the flux and polarization emerging from a $T_{\text{eff}} = 9000$ K, $\log g = 8$, line blanketed model in radiative equilibrium, taken from Wehrse (1976). The resonance absorption depresses the continuous flux spectrum in $\lambda\lambda$4000–8000 Å (dashed line), since it operates effectively in the frequency range approximately $\omega_c(H_p)$ to $\omega_c(H_p)/2$, corresponding, respectively, to the polar regions which contribute 'strongly' in the blue, and to the equatorial regions which contribute 'weakly' in the red – the reason being a reduction in field strength by a factor of 2 between the pole and the equator of a dipole field. The non-magnetic ($H = 0$) flux spectrum is shown by the dotted line for the sake of comparison. Since the 'collisionless plasma approximation' absorption coefficient (Equation (36)) has a very narrow profile its contribution is insignificant, whereas the classical 'cold plasma approximation' absorption coefficient (Equation (37)) absorbs over a large frequency band at each point on the disk. The bandwidths are quite large because the collisional damping (Equation (38)) is very strong. An extensive and systematic study of the quantum effects in cyclotron plasma absorption has been made by Pavlov *et al.* (1980a). The spectra and polarization produced in a realistic atmosphere under cyclotron mechanism are difficult to understand qualitatively when the disk integration is performed. However, certain features of the spectrum and polarization shown in Figure 5 can be understood by comparing it with Figures 2, 5, and 6 of Pavlov *et al.* (1980b). Computations using other models show that the degree and sign of polarization depend on $((\mathrm{d}/\mathrm{d}\lambda)\mathbf{A}, \mathbf{B})$ and $((\mathrm{d}/\mathrm{d}\tau)\mathbf{B})$ for a given field distribution on the stellar disk. The circular polarization $\bar{q}$ shows a strong wavelength dependence, unlike the thermal continuum polarization in weak field magnetic white dwarfs.

4. Conclusions

We have described a simplified approach, based on the earlier DSM equations, which is useful for quantitative work on stellar polarization using vector transfer equations.

The accuracy as well as the limits of applicability are pointed out. In all the problems presented above, we have obtained almost a 30% saving in computing time over the earlier procedure (Nagendra and Peraiah, 1985a) used for the same purpose. The effects of field inhomogeneities and velocity fields on the strong field Zeeman line formation are described. These effects are quantitatively more pronounced for the solar magnetic regions than those shown here for weak field magnetic white dwarfs. Collisionally-damped cyclotron absorption is stronger than expected earlier, and the saturation produced by it is responsible for the difficulty in fitting thermal energy distributions to the observed spectrum, when such a strong non-thermal phenomena is operative in magnetic stars in general and white dwarfs in particular.

Acknowledgements

One of us (K.N.N.) is grateful to Dr P. Venkatakrishnan for useful discussions.

References

Angel, J. R. P.: 1977, *Astrophys. J.* **216**, 1.
Beckers, J. M.: 1969, *Solar Phys.* **9**, 372.
Bekefi, B.: 1966, *Radiation Processes in Plasmas,* Wiley, New York.
Deguchi, S. and Watson, W. D.: 1985, *Astrophys. J.* **289**, 621.
Grant, I. P.: 1963, *Monthly Notices Roy. Astron. Soc.* **125**, 417.
Grant, I. P. and Hunt, G. E.: 1969, *Proc. Roy. Soc.* **A313**, 199.
Gnedin, Yu. N. and Sunyaev, R. A.: 1974, *Astron. Astrophys.* **36**, 379.
Heinzel, P.: 1978, *Bull. Astron. Inst. Czech.* **29**, 159.
Kalkofen, W. and Wehrse, R.: 1982a, *Astron. Astrophys.* **108**, 42.
Kalkofen, W. and Wehrse, R.: 1982b, *Astron. Astrophys.* **110**, 18.
Lamb, F. K. and Sutherland, P. G.: 1974, in C. J. Hansen (ed.), 'Physics of Dense Matter', *IAU Symp.* **53**, 265.
Landstreet, J. D. and Angel, J. R. P.: 1975, *Astrophys. J.* **196**, 819.
Landi Degl'Innocenti, E.: 1979, *Solar Phys.* **63**, 237.
Matta, F. and Reichel, A.: 1971, *Math. Comp.* **25**, 339.
Martin, B. and Wickramasinghe, D. T.: 1979a, *Monthly Notices Roy. Astron. Soc.* **189**, 69.
Martin, B. and Wickramasinghe, D. T.: 1979b, *Monthly Notices Roy. Astron. Soc.* **189**, 883.
Martin, B. and Wickramasinghe, D. T.: 1982, *Monthly Notices Roy. Astron. Soc.* **200**, 993.
Melrose, D. B.: 1980, *Plasma Astrophysics*, Vol. 1, Gordon and Breach, New York.
Nagendra, K. N. and Peraiah, A.: 1984, *Astrophys. Space Sci.* **104**, 61.
Nagendra, K. N. and Peraiah, A.: 1985a, *Monthly Notices Roy. Astron. Soc.* **214**, 203.
Nagendra, K. N. and Peraiah, A.: 1985b, *Astron. Astrophys.* (submitted).
Pavlov, G. G. and Shibanov, Yu. A.: 1978, *Soviet Astron.* **22**, 214.
Pavlov, G. G., Shibanov, Yu. A., and Yakovlev, D. G.: 1980a, *Astrophys. Space Sci.* **73**, 33.
Pavlov, G. G., Mitrofanov, I. G., and Shibanov, Yu. A.: 1980b, *Astrophys. Space Sci.* **73**, 63.
Peraiah, A.: 1984, in W. Kalkofen (ed.), *Methods in Radiative Transfer*, Cambridge Univ. Press, Cambridge.
Peraiah, A. and Varghese, B. A.: 1985, *Astrophys. J.* **290**, 425.
Staude, J.: 1970, *Solar Phys.* **15**, 102.
Stenflo, J. O.: 1971, in R. Howard (ed.), 'Solar Magnetic Fields', *IAU Symp.* **43**, 101.
Varga, R. S.: 1963, *Matrix Iterative Analysis*, Englewood Cliffs, Prentice-Hall, N.J.
Wehrse, R.: 1976, *Astron. Astrophys. Suppl.* **24**, 95.
Wickramasinghe, D. T.: 1972, *Mem. Roy. Astron. Soc.* **76**, 129.
Wiscombe, W. J.: 1976, *J. Quant. Spectros. Rad. Transfer* **16**, 477.
Wittmann, A.: 1974, *Solar Phys.* **35**, 11.